STUDY ON THE THERMAL AND MASS EVOLUTION BEHAVIOR OF METHANE AIR PREMIXED GAS UNDER RIGID AND FLEXIBLE OBSTACLES

Qixiang WANG [1,2,3], Zhigang ZHANG [2,3]*, Zhongquan LI [1], Changguo HUANG [2,3], Fengying LONG [4], Shilin LEI [5], Min CHEN [6], Zhuangzhuang YAO [2,3]

(1. College of Earth Science, Chengdu University of Technology, Chengdu, Sichuan 610059, China;

2. China Coal Technology & Engineering Group Chongqing Research Institute, Chongqing 400037, China;

3. State Key Laboratory of Gas Disaster Monitoring and Emergency Technology, Chongqing 400037, China;

4. ZNDY of Ministerial Key Laboratory Nanjing University of Science and Technology, Nanjing 210094, China;

5. National Defense College of Engineering, Army Engineering University of PLA, Nanjing 210007, China.

6. Chongqing Huadi Zihuan Technology Co., Ltd. Chongqing 400042, China)

*** Corresponding author:** ***2390561022@qq.com (Zhigang ZHANG [2,3]*)***

Abstract: There has been a lack of public reports on the combustion and explosion risks under the coupling effect of different structural materials in coal mine tunnels. Therefore, this article uses a square pipeline with a cross-section of 0.01 m^2 and a length of 1 m to study the methane combustion and explosion process under different blockage rates and rigid and flexible obstacle arrangements, in order to fully reveal the impact of tunnel construction on explosions. The results indicate that when a rigid obstacle is in the forward position, the blockage rate of a flexible obstacle is positively correlated with the flame contact velocity, maximum velocity, and maximum explosion pressure inside the pipeline. When placing a flexible obstacle in the front, as the blockage rate of the flexible obstacle increases, the contact speed and maximum speed first increase and then decrease. As the blockage rate of flexible obstacles increases, the maximum upstream explosion pressure first decreases and then increases, while the total pressure inside the pipeline first increases and then decreases. When flexible and rigid obstacles are combined and placed, they both increase heat transfer, convection, and radiation inside the tube, indirectly reducing the risk of hot air caused by explosions. Under the premise of a flexible obstacle blockage rate of 0.4, the maximum downstream overpressure can reach 2.96 times that of the upstream area, providing data support and theoretical reference for the safe layout of explosion-proof structures and equipment.

Keywords: *Coal mine; methane; flame front velocity; explosion pressure; heat and mass transfer*

1 Introduction

Coal mines continue to hold a pivotal position in the energy supply and demand systems of numerous countries [1][2], and the development of safety technologies for gas explosion prevention and control affects the progress of coal mining work. This also leads to the need for extensive research to clarify gas explosion risks and provide decision-making basis for safety prevention of explosions. There are many factors that restrict the risk of gas explosion in confined spaces such as mines. Gas is mainly composed of methane **Error! Reference source not found.**[3]. Therefore, some scholars have conducted research on the influence of methane concentration on the risk of combustion and explosion, and summarized that the maximum risk of combustion and explosion occurs when the methane concentration is 9.5% [5][6].

Subsequently, researchers investigated the impact of obstacles in mines on the evolution behavior of methane flames and overpressure. For instance, Shengnan Li [7] investigated the impact of low blockage rates on methane explosions. As the obstacle blockage rate increases, the flame propagation velocity initially surges and subsequently declines. Shen Fang [8] observed that the presence of obstacles causes the center of the flame's leading edge to deform and bulge after adopting a hemispherical shape, ultimately evolving into a bundled flame. Notably, in the absence of a tulip flame, when the blockage ratio (BR) equals 0.5, the flame reaches the obstacle's position first. Additionally, Qiao Zhenglong [9] discovered that as the gradient of the blockage ratio increases, the time taken for the flame to propagate to the pipeline's end also increases, resulting in the formation of a flocculent flame at the pipeline's termination. Wu Qifen [10] found that during the combustion of non-uniform mixtures, a triple flame structure emerges, and its manifestation delays as the obstacle position shifts further. The highest velocity of the flame's leading edge and the maximum overpressure value were recorded at an obstacle position of 400mm [11][12].

As research delves further, attention is directed towards the structural characteristics of obstacles, categorizing them into rigid and flexible structures based on their ability to resist deformation under pressure and flame impact within the explosion field. Zheshi Wang [13] observed that an augmentation in the thickness of flexible obstacles augments the flame propagation velocity, which in turn elevates turbulence intensity and explosion severity. Yu Shuwei and Duan Yulong [14][15] discovered that as the blockage ratio of flexible obstacles increases, the maximum flame and explosion pressure exhibit a trend of initial increase followed by a decrease, mirroring the behavior observed with rigid obstacles. Gao Ke [16] noted that the presence of flexible obstacles on pipes tends to induce numerous wrinkles in the flame shapes. Li Quan [17] found that significant deformation of flexible obstacles, accompanied by a corresponding reduction in blockage ratio, led to a decrease in the velocity of the flame tip as it traversed the obstacle. This deformation also constrained the development of vortices and intense shear layers in downstream areas. Furthermore, the facilitating effect of flexible obstacles on the rate of flame spread and pressure rise was found to be lesser compared to that of rigid obstacle.

In reality, explosive accidents frequently lead to the coexistence of flexible and rigid structures in confined space, such as flexible pipelines and beam structures in coal mine tunnels, underground fire doors and concrete columns, etc. Despite the aforementioned studies having examined the combustion characteristics of methane gas in the presence of obstacles possessing single properties, there remains a notable gap in exploring the combustion disaster effects that

arise when flexible and rigid structures coexist. In light of this, the advancement of this project can offer valuable insights to scholars engaged in future fundamental research endeavors, and further provide essential data support and theoretical guidance for the planning and layout of relevant safety facilities.

2 Experimental methods

2.1 Experimental Equipment

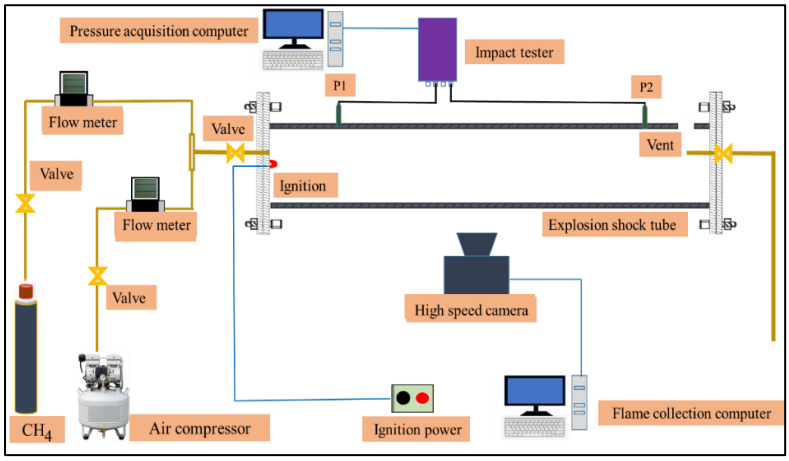

Figure 1 Experimental device

The explosion experimental device in **Figure 1**, explosion pipeline is fashioned as a rectangular prism, measuring 1 m in length and featuring equal width and height dimensions of 10 cm. The supply and exhaust system encompasses mass flow meters, methane cylinders, air compressors, gas conduits, and exhaust lines. The methane gas used has a purity of 99%, with both the gas and exhaust conduits having an internal diameter of 1 cm. The system necessitates two mass flow meters, each with a flow rate range of 0-5 L/min. The flame acquisition setup includes a high-speed camera (Phantom V710L) and a flame acquisition host equipped with PCC 3.6 software, configured with a sampling frequency of 2000 fps, an exposure time of 500 μs, and a resolution of 1280 × 240 pixels. The pressure acquisition system consists of a high-pressure shock wave tester (Blast PRO), set with a sensitivity coefficient of 0.1%, a sampling frequency of 50 kHz, and pressure acquisition software (Tytest Data View). Additionally, two PCB piezoelectric pressure sensors are utilized. For the safety of the experimental apparatus, a 2.5 cm diameter explosion vent is positioned on the right side, sealed with a thin PVC film during operational procedures. The rigid obstacle is constructed from a carbon fiber board, while the flexible obstacle is made of polyurethane foam that has been impregnated with flame retardant liquid and then dried to minimize experimental errors stemming from spontaneous combustion of the materials [18].

2.2 Experimental Procedure

Assemble the explosion testing apparatus, including the explosion pipeline and methane cylinder, as illustrated in **Figure 1**. Conduct ignition tests to verify the proper functionality of the ignition system. Position the rigid and flexible obstacles respectively at their designated locations (40 cm and 50 cm) [19]. Adjust the methane and air mass flow meters to the desired settings, and

activate the air compressor to introduce air directly into the pipeline. Purge the experimental pipeline of impurities for a duration of 1-2 minutes. Upon completion of purging, securely seal the explosion vent using a PVC film. Chen C [20] concluded that when the obstacle blocking rate is 0.4, the explosion pressure can reach its maximum. Repeat the air introduction process and verify the pipeline's airtightness by inspecting the PVC film for any bulging. Introduce methane gas according to the specifications outlined in **Table 1**. Employ the 4-fold volume method to ventilate the pipeline for 8 minutes, followed by a minute rest period after ventilation. This ensures thorough mixing of the two gases during the ventilation process. Initiate the ignition trigger, simultaneously activating the acquisition devices and software for pressure and flame image data collection. Prior to conducting the next set of experiments, open the exhaust valve and use air to clear the interior of the pipeline. Each experimental condition should be tested a minimum of three times to control experimental errors.

Table.1 Experimental conditions

Case	Methane volume fraction	Air volume fraction	Obstacle distance from explosion source	
			40 cm	50 cm
1	9.5%	90.5%	BRR_{igid} = 0.2	$BR_{Flexible}$= 0.2
2				$BR_{Flexible}$= 0.4
3				$BR_{Flexible}$= 0.6
4			$BR_{Flexible}$= 0.2	
5			$BR_{Flexible}$= 0.4	BR_{Rigid} = 0.2
6			$BR_{Flexible}$= 0.6	

3 Results and Discussion

3.1 Flame Evolution Behavior

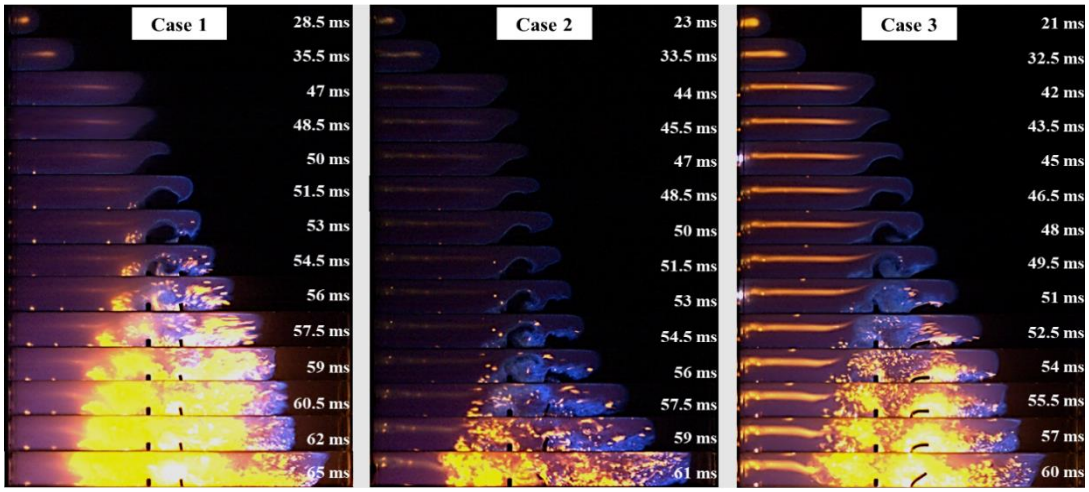

(a) (b) (c)

Figure 2 Flame behavior in front of rigid obstacle

Figure 2 illustrates the temporal evolution of the flame in the presence of a rigid obstacle positioned upfront. Examining **Figure 2**, it becomes evident that, with a rigid obstacle blockage

ratio of 0.2 in the forward position, the flame front undergoes a generally similar shape transformation in its initial phase, characterized by distinct spherical flames at 28.5 ms, 23 ms, and 21 ms, followed by finger-shaped flames at 35.5 ms, 33.5 ms, and 32.5 ms. As the flame front traverses above the rigid obstacle (40 cm), the upper flame front exhibits a stretching phenomenon, which becomes increasingly pronounced as the blockage ratio of a flexible obstacle increases from 0.2 to 0.6. During the flame's propagation, flame vortices also emerge at the flame tip. Furthermore, **Figure 2** reveals that notable flame vortices form between the rigid and flexible obstacles at a blockage ratio of 0.2 and at 56 ms. When the blockage ratio rises to 0.4 and 0.6, the emergence of flame vortices at the same location is delayed by 1.5 ms and 6.5 ms, respectively. The transmission times of the flame tip to the explosion vent in these three scenarios are 65 ms, 61 ms, and 60 ms, respectively. This suggests a positive correlation between the flame front propagation velocity and the blockage ratio of flexible obstacles. An increase in the height of flexible obstacles triggers an acceleration mechanism for flame propagation. This is due to the weakening of the obstacles' ability to maintain their shape as the blockage ratio increases. The tilting state of flexible obstacles is closely related to the high-pressure environment formed between two types of obstacles. As the blocking rate of flexible obstacles increases, more fuel accumulates between the two, resulting in higher pressure and impact effects. Therefore, the right leaning effect of flexible obstacles is clearly observed when the obstacle is 0.6, thereby intensifying the forward propagation of shock waves and flames and influencing the fluid disturbance within the pipeline.

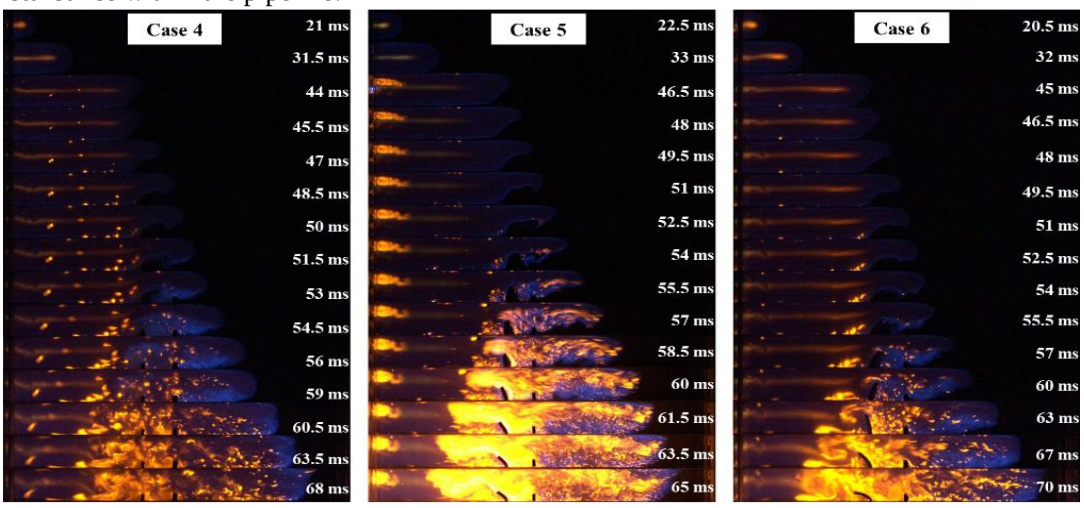

(a) (b) (c)

Figure 3 Flame behavior of flexible obstacle are placed in front

Figure 3 displays the flame evolution process under three operational scenarios, with a flexible obstacle pre-positioned. The flame front's shape transformation aligns with that observed in Figure 2. However, when the blocking ratios of both obstacles are equivalent, spherical flame formation occurs 7.5 ms earlier in Case 4 compared to Case 1, 0.5 ms earlier in Case 5 versus Case 2, and 0.5 ms earlier in Case 6 compared to Case 3. This suggests a declining trend in the time required for the emergence of spherical and finger-shaped flames as the blockage ratio of the flexible obstacle increases. In **Figure 3**, no significant flame vortices are observed between rigid and flexible obstacle. This is attributed to the impact of the flame and pressure shock wave on the

flexible obstacle positioned upfront, causing it to bend and primarily tilt to the left. The reason is affects the fluid disturbance and establishes a negative feedback mechanism that inhibits the formation of flame vortices. Notably, the time taken to reach the venting port increases compared to scenarios with a rigid obstacle alone, recording 68 ms, 65 ms, and 70 ms respectively. The time consumption exhibits a trend of initial decrease followed by increase with the augmentation of the flexible obstacle's blockage ratio. This pattern contrasts with the development of spherical and finger-shaped flames during the initial stage.

This discrepancy diverges from the currently understood positive feedback mechanism associated with methane combustion and thermal diffusion efficiency. While flexible obstacle do enhance combustion efficiency by accelerating the process, variations in their blockage ratio lead to differing combustion efficiencies. Consequently, flexible obstacles play a pivotal role in numerous explosion-related fields.

3.2Variation of flame front velocity

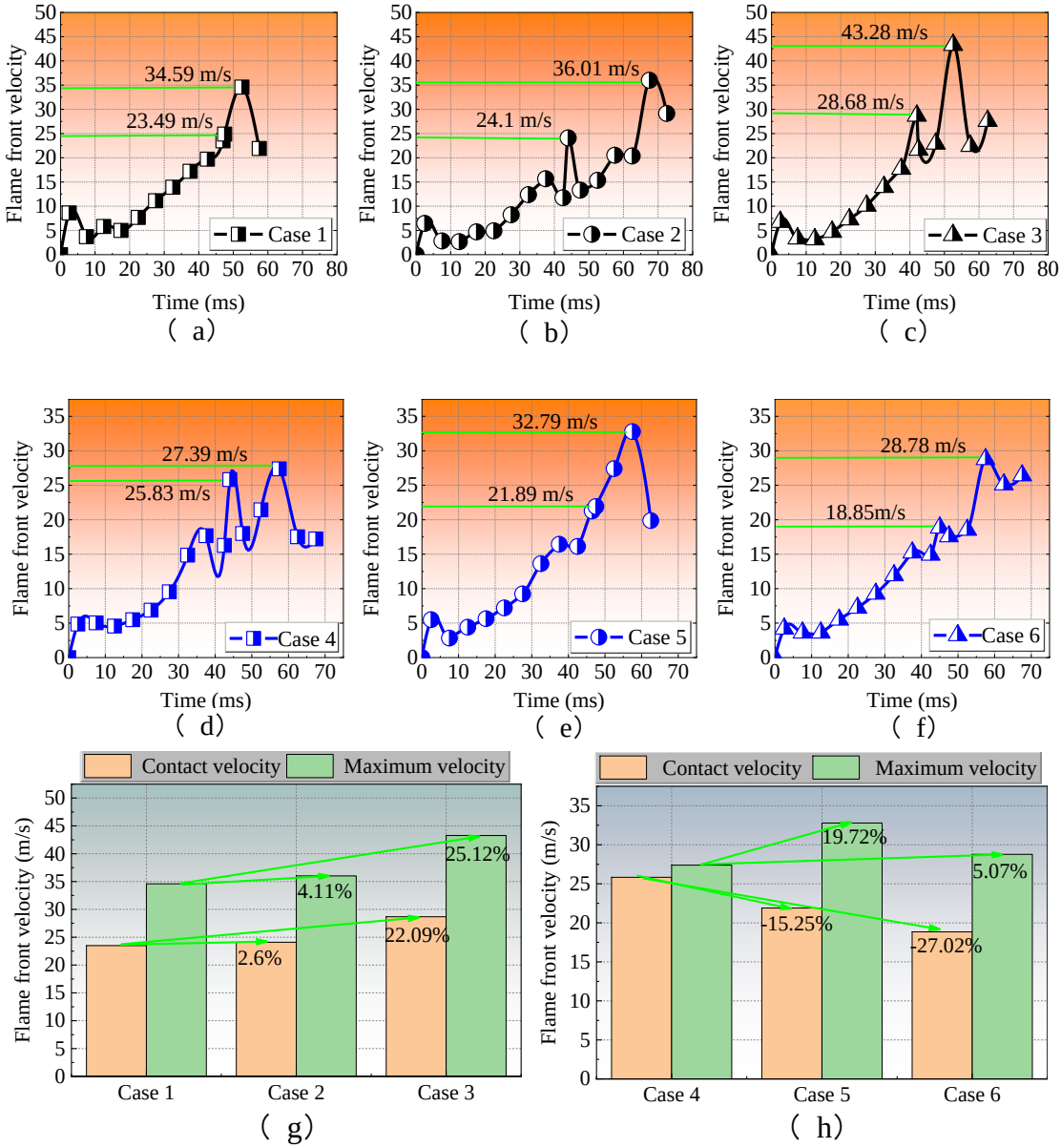

Figure 4 Flame forward propagation velocity under different conditions

Based on the flame presented in **Figure 2** and **Figure 3**, a time step of 5 ms was selected to compute the motion velocity of the flame front, serving as an indicator of flame propagation velocity. Specifically, the velocity at which the flame front reaches the first obstacle is termed the "contact velocity," while the peak velocity achieved during the entire propagation process is designated as the "maximum velocity." The product of velocity and mass is the magnitude of momentum, so the contact velocity at an obstacle represents the magnitude of the impact of momentum on the obstacle in this environment. The maximum speed represents the speed of flame propagation that can be caused in this obstacle placement environment, which provides a reference for protective structures. **Figure 4** illustrates the variations in flame velocity under different operational scenarios, spanning from **Figure 4(a)** to **(f).** Examining **Figure 4**, it becomes evident that in the presence of rigid obstacles upfront, as the blocking ratio of flexible obstacles situated in the rear increases, both the contact velocity and maximum velocity exhibit a positive correlation with this blocking ratio. For instance, in Case 1, the contact velocity and maximum velocity were recorded at 23.49 m/s and 34.59 m/s, respectively. As the blocking ratio of the flexible obstacle rose to 0.4, the contact velocity increased by +2.6%, and the maximum flame velocity augmented by +4.11%. Furthermore, when the blocking ratio climbed to 0.6, these velocities surged by +22.09% and +25.12%, respectively.

In the context of flexible obstacle pre-placement, there exists a disparity between the variations observed in contact velocity and maximum velocity. Specifically, the contact velocity exhibits a consistent decline as the blockage rate of flexible obstacles increases, whereas the maximum velocity follows a trend of initial increase followed by a decrease with rising blockage rates. In Case 4, the contact velocity and maximum velocity were measured at 25.83 m/s and 27.39 m/s, respectively. As the obstruction rate of flexible obstacles rose to 0.4 and 0.6, the contact velocity changed by -15.25% and -27.02%, respectively, while the maximum velocity increased by +19.72% and +5.07%, respectively. For the reason that, in scenarios where a flexible obstacle precedes, the contact velocity is assessed above the obstacle. The flame velocity is not only related to the combustion pressure, but also closely related to the airflow field inside the tube. The bending and tilting process of flexible obstacles carries a certain speed. Therefore, when the flame propagates forward, the presence of flexible obstacles that move at a velocity to the left will cause the airflow to flow rapidly upstream, indirectly reducing the flame velocity. As the blockage rate of the flexible obstacle escalates, the disturbance to flame propagation intensifies, causing a sustained decrement in velocity. Regarding the trend of maximum velocity variation, the bending effect of flexible obstacles is less pronounced at a blockage rate of 0.4 compared to 0.6. However, it should be clarified that at this juncture, the actual blockage ratio of flexible obstacles within the explosion field surpasses 0.6, significantly exceeding the blockage rate observed at 0.2.

3.3 Variation of explosion overpressure

Figure 5 shows the temporal variation of pressure in both the upstream and downstream sections of the pipe when a rigid obstacle is positioned at the forefront, whereas **Figure 6** depicts the scenario with a flexible obstacle in front. Upon scrutinizing both figures, it becomes evident that, in the upstream region, from the inception to the point of maximum explosion pressure attainment, a negative pressure condition persists. In the case, this negative pressure escalates as

the flexible obstacle's blockage rate increases. Conversely, the scenario depicted in **Figure 6,** where a flexible obstacle precedes, the negative pressure exhibits a pattern of initial increase followed by a decrease with the rising blockage rate of the flexible obstacle. This phenomenon suggests that regardless of whether flexible obstacles are positioned upstream or downstream of the pipe, they introduce varying levels of airflow disruption, ultimately resulting in a substantial consumption of fuel and air in the upstream area within a brief timeframe. Consequently, this leads to a decrement in upstream pressure. The fluctuation in negative pressure can further be attributed to the enhanced gas disturbance caused by the flexible obstacles, which in turn accelerates the consumption of fuel and air in the upstream vicinity.

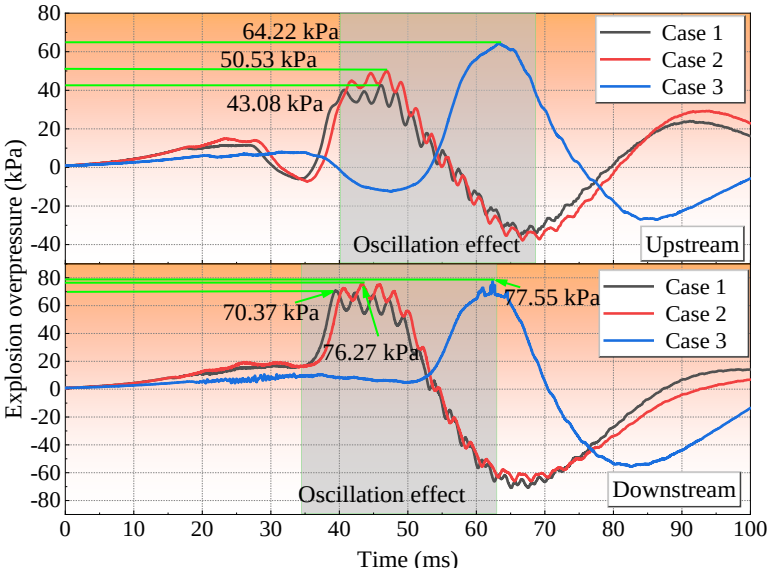

Figure 5 Explosion overpressure curve of rigid obstacle are placed in front

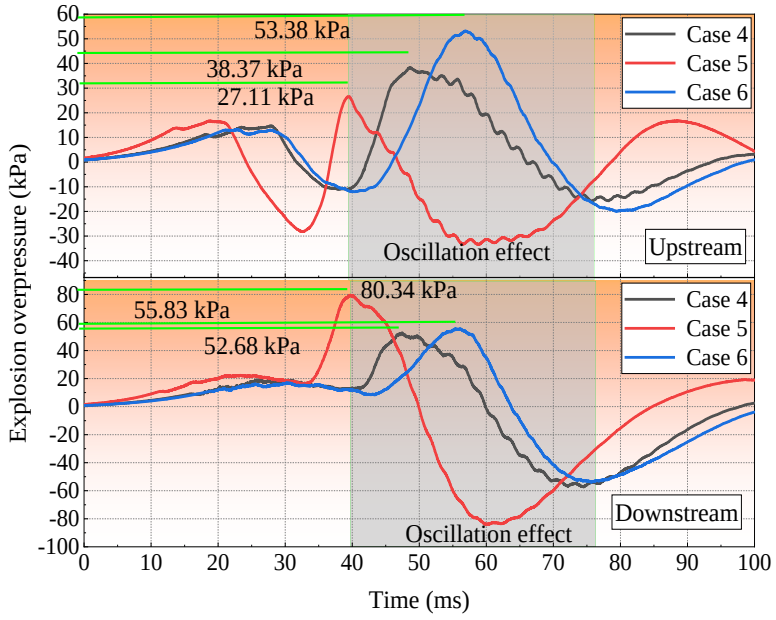

Figure 6 Explosion overpressure curve of flexible obstacle are placed in front

For the maximum explosion pressure, in the case of pre installation of rigid obstacles, the

maximum explosion pressure will also increase with the increase of the blocking rate of flexible obstacles. Specifically, for Case 1, the upstream and downstream pressures are recorded as 43.08 kPa and 70.37 kPa, respectively. As the flexible obstacle's blocking rate escalates to 0.4, the upstream pressure undergoes a +17.29% increase, while the downstream pressure experiences a +8.38% surge. However, when the blocking rate reaches 0.6, the upstream pressure undergoes a substantial +49.07% increase, and the downstream pressure rises by +10.2%, as illustrated in **Figure 7(a)**. Conversely, in Case 4, the maximum explosion pressures upstream and downstream are noted as 38.37 kPa and 52.68 kPa, respectively. As the flexible obstacle's blocking rate increases, the upstream maximum explosion pressure undergoes a -29.35% decrease at a blocking rate of 0.4, but then reverses to a +39.12% increase at a blocking rate of 0.6. The downstream maximum explosion pressure, on the other hand, exhibits an initial +52.51% increase at a blocking rate of 0.4, followed by a more modest +5.98% increase at a blocking rate of 0.6. Notably, the upstream maximum explosion overpressure demonstrates a trend of initial decrease followed by an increase with the rising flexible obstacle blocking rate, whereas the downstream maximum explosion overpressure exhibits an opposite trend—increasing initially and then decreasing. At a specific blockage rate of 0.4, the difference in pressure evolution behavior can be attributed to the intensified disturbance of the flow field inside the pipe by the flexible obstacle, while different shock wave evolution behaviors lead to changes in the instantaneous actual blockage rate of the flexible obstacle at a certain moment. The interaction between these two mechanisms results in that when the actual blockage rate in the explosion field exceeds 0.6 and 0.2, the magnitude of the actual blockage rate helps to facilitate sufficient interaction between the micro porous units of the flexible obstacle and the flame and heat, resulting in lower pressure in the upstream region than observed at blockage rates of 0.2 and 0.6. In addition, the intensified disturbance enhances the transport of airflow and heat downstream in the pipeline, forming a continuous obstacle mechanism together with rigid obstacles behind the pipeline. This mechanism is more effective than those observed at blockage rates of 0.2 and 0.6, resulting in higher downstream fuel consumption rates and greater explosion overpressure.

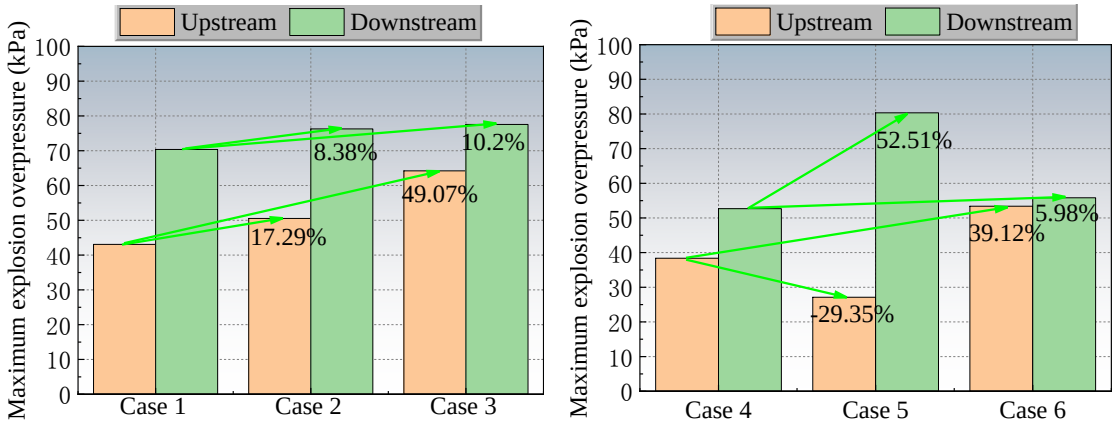

(a) (b)

Figure 7 Comparison of maximum explosion overpressure

Observing **Figure 5** and **Figure 6**, it becomes evident that when the explosion overpressure

attains its peak, it subsequently initiates a decline, a process invariably accompanied by oscillatory effects. An evaluation of the overpressure curves in both the upstream and downstream regions, under 6 conditions, reveals a notable pattern: as the blockage rate of flexible obstacles increases, the oscillation phenomenon diminishes. This suggests that an augmentation in the blockage rate of flexible obstacles leads to a reduction in the pressure amplitude within the pipeline. In addition to comparing the peak explosion pressures within the pipeline, another crucial consideration for explosion hazard prevention and control lies in the disparity between the maximum explosion pressures in the upstream and downstream regions under the same obstacle arrangement (**Figure 7**). When comparing the maximum explosion overpressures upstream and downstream for two different obstacle arrangements, it was discovered that Case 5 exhibited the largest difference, with the downstream maximum explosion pressure being 2.96 times greater than that of the upstream area. Consequently, the strategic placement of explosion-proof structures and equipment facilities is of paramount importance.

3.5 Exploration of Heat and Mass Transfer Mechanism in Flame Propagation Process

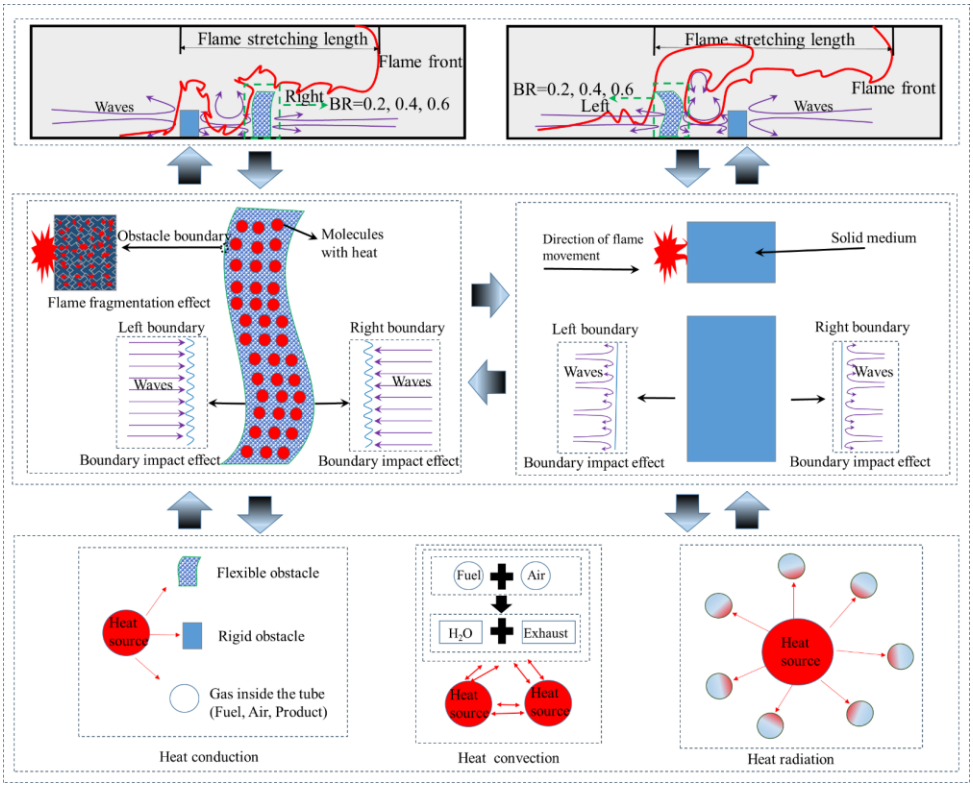

Figure 8 Analysis of the process of heat and mass transfer

Figure 8 analyzes the rigid and flexible obstacles in the explosion field and their impact on shock waves and flame changes. The evolution behavior of methane explosion flames under the front of rigid and flexible obstacles mainly lies in three aspects: Firstly, it is the main bending direction of flexible phase obstacles, with the main bending direction of rigid obstacles being to the right and that of flexible obstacles being to the left when they are in front. Secondly, It is the stretching of flames, and the stretching effect produced by the flexible obstacle in front of it is more pronounced. There is a significant difference in the changes exhibited by obstacles arranged in two different ways within the tube. Firstly, this is reflected in the flame quenching mechanism

obstructed by the left and right boundaries. The boundary of flexible obstacles can generate flame fragmentation effects, leading to the contact between the small gap skeleton of flexible obstacles and flame heat. Rigid obstacles completely block the propagation of flames, inducing the flame tip to move slowly in the opposite direction. Secondly, there is the influence of shock waves. The surface of flexible obstacles is affected by the impact, resulting in surface irregularities and uneven force distribution, leading to overall bending and tilting effects of the flexible obstacles. Rigid obstacles completely reflect the shock wave, so the flame folds are more pronounced when the rigidity is in front[19][20]. Finally, Overall, flexible obstacles, regardless of whether they are placed in front or not, will intensify methane combustion and generate heat [21]. The heat will intensify the flow, which in turn promotes more combustion. Promotes heat convection and conduction inside the tube, accelerates heat diffusion, and further induces a stronger heat radiation conduction mechanism, which also increases heat consumption.

4 Conclusion

(1) When a rigid obstacle is positioned upfront, the flame contact velocity, maximum velocity, and maximum explosion pressure all peak at a flexible obstacle obstruction rate of 0.6, registering values of 28.68 m/s, 43.28 m/s, and 77.55 kPa, respectively. A positive correlation is observed between the blocking rate of flexible obstacles and various flame characteristics, including the velocity of flame propagation, flame contact velocity, maximum velocity, and maximum explosion pressure.

(2) The initial phase of flame propagation undergoes a gradual deceleration when a flexible obstacle is positioned upfront, effectively dampening the formation of internal vortices. The flame contact velocity decreases progressively as the blockage rate of the flexible obstacle increases, peaking at 25.83 m/s when the obstruction rate is 0.2. However, both the maximum flame velocity and the maximum explosion overpressure exhibit a trend of initial increase followed by a decrease as the blockage rate of flexible obstacles rises, ultimately reaching values of 32.79 m/s and 80.34 kPa, respectively.

(3) Compared the hazards of the maximum overpressure difference between upstream and downstream under two different obstacle arrangements, the maximum overpressure difference occurs in the pre working condition with a flexible obstacle blockage rate of 0.4. At this time, the maximum overpressure downstream can reach 2.96 times that of the upstream area. Consequently, the strategic placement of explosion-proof structures and equipment necessitates thorough consideration of the upstream and downstream maximum pressure-bearing capacities in relation to explosion risks.

Acknowledgements

This work was supported by the National Key Research and Development Program of China, (2023YFC3009003); Natural Science Foundation of Chongqing, China (CSTB2024NSCQ-MSX0010). Thanks.

Reference

[1] Bibler C J, Marshall J S, Pilcher R C. Status of worldwide coal mine methane emissions and use[J]. International Journal of Coal Geology, 1998, 35(1-4): 283-310.

[2] Zhou F, Xia T, Wang X, et al. Recent developments in coal mine methane extraction and utilization in China: a review[J]. Journal of Natural Gas Science and Engineering, 2016, 31: 437-458.

[3] Song Q, Xiao R, Li Y, et al. Catalytic carbon dioxide reforming of methane to synthesis gas over activated carbon catalyst[J]. Industrial & engineering chemistry research, 2008, 47(13): 4349-4357.

[4] Balcombe P, Anderson K, Speirs J, et al. The natural gas supply chain: the importance of methane and carbon dioxide emissions[J]. ACS Sustainable Chemistry & Engineering, 2017, 5(1): 3-20.

[5] Wang Q, Jin S, Luo Z, et al. Flame propagation characteristics of methane explosion under different venting conditions[J]. Fuel, 2023, 334: 126721.

[6] Shen X, Zhang B, Zhang X, et al. Explosion characteristics of methane-ethane mixtures in air[J]. Journal of Loss Prevention in the Process Industries, 2017, 45: 102-107.

[7] Li S, Gao K, Xia H, et al. Effect of low blockage ratio obstacle on explosion characteristic in methane/air mixture[J]. Arabian Journal of Chemistry, 2024, 17(9): 105890.

[8] Shen F, Wen X, Zhang S, et al. Effect of square-hole obstacle in a long pipe on methane/air premixed explosion characteristics[J]. Energy Sources, Part A: Recovery, Utilization, and Environmental Effects, 2023, 45(4): 12808-12820.

[9] Qiao Z, Ma H, Li C. Influence of change in obstacle blocking rate gradient on LPG explosion behavior[J]. Arabian Journal of Chemistry, 2023, 16(2): 104496.

[10] Wu Q, Yu M, Zheng K. Experimental investigation on the effect of obstacle position on the explosion behaviors of the non-uniform methane/air mixture[J]. Fuel, 2022, 320: 123989.

[11] Xiao G, Wang S, Mi H, et al. Analysis of obstacle shape on gas explosion characteristics[J]. Process Safety and Environmental Protection, 2022, 161: 78-87.

[12] Zuo Q, Wang Z, Zhen Y, et al. The effect of an obstacle on methane- air explosions in a spherical vessel connected to a pipeline[J]. Process safety progress, 2017, 36(1): 67-73.

[13] Wang Z, Zhang Z, Yu J, et al. The effect of flexible obstacles with different thicknesses on explosion propagation of premixed methane-air in a confined duct[J]. Heliyon, 2023, 9(8): e18803-e18803.

[14] Yu S, Duan Y, Long F, et al. The influence of flexible/rigid obstacle on flame propagation and blast injuries risk in gas explosion[J]. Energy Sources, Part A: Recovery, Utilization, and Environmental Effects, 2023, 45(2): 4520-4536.

[15] Duan Y, Long J, Yu S, et al. Mechanism of accelerating premixed hydrogen/methane flame with flexible obstacles[J]. International Journal of Hydrogen Energy, 2024, 64: 1021-1029.

[16] Gao K, Li S, Liu Y, et al. Effect of flexible obstacles on gas explosion characteristic in underground coal mine[J]. Process Safety and Environmental Protection, 2021, 149: 362-369.

[17] Li Q, Ciccarelli G, Sun X, et al. Flame propagation across a flexible obstacle in a square cross-section channel[J]. International Journal of Hydrogen Energy, 2018, 43(36): 17480-17491.

[18] Lei S, Duan Y, Long J, et al. Study on the effects of elastic modulus of constructions on heat and mass transfer of gas explosion[J]. Thermal Science, Vol.28 (2024) 3B, pp: 2693-2702 .

[19] Duan Y, Lei S, Li Z, et al. Study on flexible/rigid protection mechanism of hydrogen/methane premixed gas explosion in urban underground space[J]. Process Safety and Environmental Protection, 2024, 182: 808-822.

[20] Chen C, Zhang Y, Zhao X. Effect of obstacle blockage ratio on deflagration characteristics of

combustible liquid vapor in channel-like structure[J]. Journal of Central South University(Science and Technology), 2022, 53(7): 2746−2755.

[21] Wen X, Guo Z, Wang F, et al. Experimental study on the quenching process of methane/air deflagration flame with porous media[J]. Journal of Loss Prevention in the Process Industries, 2020, 65: 104121.

Submitted: 5.09.2024.
Revised: 24.10.2024.
Accepted: 07.12.2024.